Growth of Co Layers on Cu(111) Studied by Forward-Focusing Angle-Resolved X-Ray Photoemission Spectroscopy and Real-Space Imaging

C. M. Wei, T. C. Zhao, and S. Y. Tong

Department of Physics and Laboratory for Surface Studies, University of Wisconsin–Milwaukee, Milwaukee, Wisconsin 53201.

(Received 9 July 1990)

We show how the intensity enhancement of angle-resolved x-ray photoelectrons along the emitter-scatterer internuclear directions can be used to monitor layer-by-layer growth of Co on Cu(111). Specifically, we show how the technique can distinguish between fcc or hcp growth and determine precisely the thickness at which the fcc stacking switches to hcp. We also show how the interference patterns around each forward-focusing direction can be used to produce real-space images of nearest-neighbor atoms in the atomic plane above the emitting atom.

PACS numbers: 79.60.Cn

The forward scattering of high-energy Auger or x-ray-excited electrons by the (attractive) atomic core potentials of a solid in the near surface region has found many applications.[1-7] The intensity enhancement is the strongest at scattering angle $\theta_s=0°$ (i.e., along the emitter-scatterer internuclear direction). This enhancement is called the forward-focusing effect[8,9] and for electrons above 300 eV, the forward-direction enhancement is almost independent of energy. (There is actually a very slow dependence on the electron's energy and forward focusing will vanish at $E\rightarrow\infty$.[10]) In this paper, we shall show how the focusing peaks can be used to distinguish between fcc or hcp stacking in the growth of Co layers in Cu(111). We shall show that the technique provides unambiguous layer-by-layer monitoring of the stacking sequence, and can determine precisely the thickness at which the fcc stacking switches to hcp. We shall also utilize the strong forward-scattering peaks to produce real-space images of the nearest-neighbor atoms in the atomic plane *above* the emitting atom.

Holographic reconstruction of diffraction patterns has been demonstrated for photoelectron diffraction[11] and diffuse low-energy electron diffraction.[12] To reduce multiple scattering, the previous studies used diffraction patterns formed by backscattered electrons at 400–550 eV energies. At such energies, the backscattered diffraction patterns are very weak. By comparison, the forward-scattering angular distributions used in this work (Co $2p_{3/2}$, $E_k=703$ eV) are over an order of magnitude stronger.

For the simulation of Co layer growth, we use a multiple-scattering slab method which includes energy-dependent photoelectron excitation matrix elements.[13,14] In this case, transitions from $p\rightarrow d$ and $p\rightarrow s$ channels are included. A p-polarized light (Al $K\alpha$ radiation) with wave vector pointing 70° from the emission direction is used and the crystal is rotated to yield the full angular scans.

At one-monolayer (ML) Co coverage, it is reasonable to place the Co atoms at the fcc continuation sites. The angular scan at 1 ML is structureless, due to the absence of forward-focused peaks. At 2-ML Co coverage, we first place the Co atoms at the fcc continuation sites: i.e., a stacking sequence of *ABCab*. Here, *A* or *a* denotes the registry of the substrate (Cu) or overlayer (Co) atoms, respectively. The full angular scan of the fcc Co x-ray photoemission spectroscopy (XPS) pattern is shown in Fig. 1, upper left. There are evident four sets of forward-focused peaks, at polar angles $\theta=35.3°$, 54.7°, 61.9°, and 68.6°, respectively (gold-colored spots). The polar angles are measured from the surface normal. A schematic diagram of the emitting atom in layer 2 and the scattering atoms in layer 1, as well as the internuclear directions, are shown in Fig. 2(a). If we then place the Co atoms in the hcp arrangement, i.e., *ABCac*, all the focusing peaks rotate in ϕ by 60° (see Fig. 1, upper right). This corresponds well with the fact that the angular relationship between the emitter and the scatterers is 60° rotated in ϕ when switching from fcc to hcp stacking. Thus, there is a one-to-one correspondence between the layer stacking sequence and the ϕ orientation of the focusing peaks.

The XPS angular scan can be integrated in $\hat{\mathbf{k}}$ space to produce real-space atomic images. Thus, to obtain holographic images,[11,12] we write

$$\phi(\mathbf{r})=\int\chi(\theta,\phi)e^{ik\hat{\mathbf{k}}\cdot\mathbf{r}}d\Omega\,. \tag{1}$$

Here, $\chi(\theta,\phi)=I(\theta,\phi)/I_D(\theta,\phi)-A$, where $I_D(\theta,\phi)$ is the intensity of the unscattered wave. In a typical experiment, $I_D(\theta,\phi)$ may be replaced by an average background intensity. A is the angle-averaged value of $I/I_D(\theta,\phi)$. Since $k^2d\Omega=d\mathbf{k}_\parallel/\cos\theta$, therefore, the real-space image is given by

$$\phi(x,y,z)=\frac{1}{k^2}\int\frac{\chi(\theta,\phi)}{\cos(\theta)}e^{ik\hat{\mathbf{k}}\cdot\mathbf{r}}dk_x\,dk_y\,. \tag{2}$$

For 2 ML, we can obtain the images of nearest-neighbor atoms in the top Co layer by setting z equal to the Co interlayer spacing. The atomic images are shown in Fig. 1,

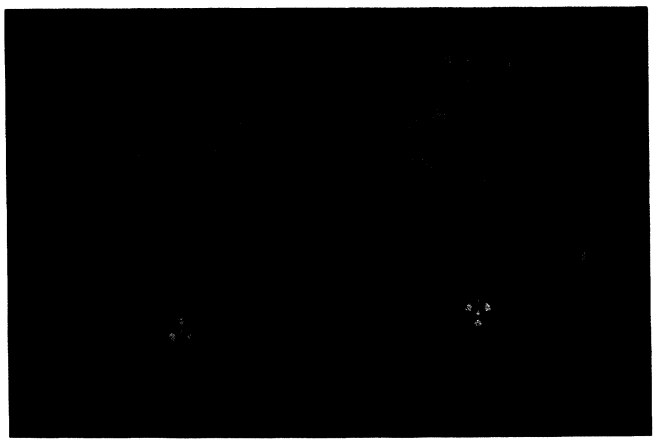

FIG. 1. Angular XPS profiles are shown in the upper panels. The focusing peaks are gold colored. The polar and azimuthal directions are shown in Fig. 2(a). Atomic images are shown in the lower panels, in red color. The vertical white bars equal 1 Å in real space.

lower left and lower right for the fcc and hcp cases, respectively. For fcc, three bright images (red spots furthest from the center) form an upright triangle. They correspond well with the positions and distances of the first-layer atoms shown in Fig. 2(a). The lateral resolution is ~ 1 Å. For the hcp structure (Fig. 1, lower right), the triangle of the atomic images is inverted, as it should be. The bright features in the center for $r \leq 0.8$ Å are noise introduced by the very limited range of k_x and k_y.

The angular scans for 3-ML Co arranged in the fcc

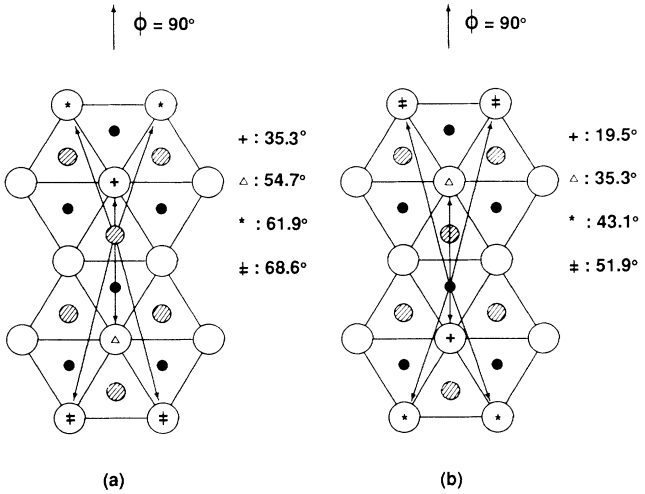

FIG. 2. Top view of internuclear focusing directions for (a) 2-ML and (b) 3-ML fcc Co layers. First, second, and third layer atoms are in decreasing sizes. The arrows point from emitter to scatterer. The polar angles are noted on the right of each figure.

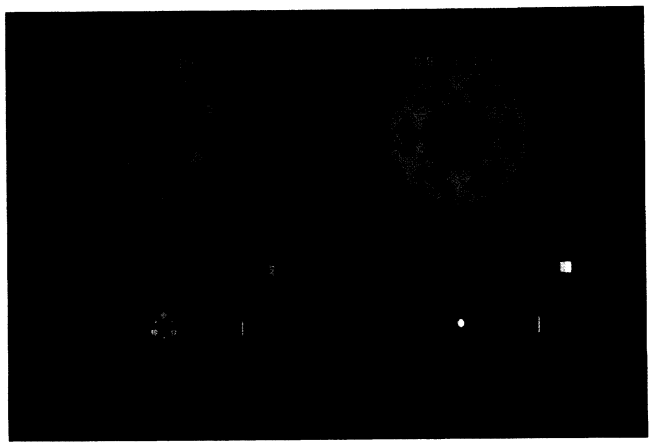

FIG. 3. Angular profiles and real-space images for 3-ML Co on Cu(111). The polar and azimuthal directions are shown in Fig. 2(b). Other conditions same as in Fig. 1.

(*ABCabc*) and hcp (*ABCaba*) stacking sequences are shown in Fig. 3, upper left and upper right, respectively. In the fcc case, besides the forward-focused peaks from $2 \rightarrow 1$ (i.e., emitter in layer 2, scatterer in layer 1), new focusing peaks appear at $\theta = 19.5°$ (set of 3), 43.1° (set of 6), and 51.9° (set of 6). Figure 2(b) provides a top view of these new focusing directions. A side view, along the $\phi = 90°$ cut, is shown in Fig. 4. The new focusing directions are due to $3 \rightarrow 1$ events (i.e., emitter in layer 3, scatterer in layer 1). Combining the two sets of focusing peaks, we can account for every major feature in the angular profile of Fig. 3, upper left. Forward-scattering peaks along non-close-packed directions have an elongated shape due to interference from the scattering of nearby atoms that do not lie along the internuclear directions.

The angular scan of the hcp stacking (Fig. 3, upper right) is significantly different. Referring to this figure, we see a pseudosixfold pattern with six bright features (gold colored) along $\theta = 35.3°$. With the Co layers in

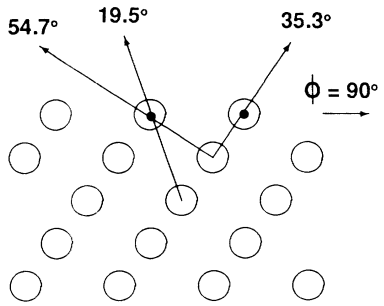

FIG. 4. Side view of fcc Co layers, showing focusing directions for emissions from layers 2 and 3 along the $\phi = 90°$ and 180° azimuths.

aba stacking, the angular orientations of the $2 \rightarrow 1$ and $3 \rightarrow 2$ focusing directions are $\phi = 60°$ rotated from one another. Specifically, $2 \rightarrow 1$ focusing produces three bright features forming the inverted triangle, and $3 \rightarrow 2$ focusing produces the features forming the upright triangle. It is in fact possible to identify the focusing directions that produce the lobelike features in the pattern, and such analyses will be reported elsewhere.[15]

The real-space images at z cut equal to one Co interlayer spacing are shown in Figs. 3, lower left and lower right, respectively, for 3-ML Co on Cu(111). For the fcc structure, the Co layers are stacked in the same orientation; hence, we see a reinforced three-atom image. Noise is increased, because inequivalent source waves are present. The emitter can be in either layer 2 or layer 3, and these are inequivalent. Also, multiple scattering (or defocusing)[9] along close-packed directions increases the noise of the $\hat{\mathbf{k}}$ transform for emissions from layers 3 or deeper.[15]

For the corresponding hcp case, the images of three neighboring atoms forming an upright triangle are produced from $3 \rightarrow 2$ focusing events, similar to that of the fcc 2-ML situation. In addition, the $2 \rightarrow 1$ focusing events produce three atomic images forming an inverted triangle (analogous to the hcp 2-ML case). However, the latter atomic images are split due to interference from $3 \rightarrow 1$ scatterings.[15] The resulting real-space image is a ring of 6 atoms, three of which are split. This is a consequence of having inequivalent source waves.

Angular profiles of thicker layers in fcc stacking, e.g., *ABCabca*... have similar threefold patterns. The case of 4-ML Co on Cu(111) is shown in Fig. 5, left. No new peaks are introduced, except that along non-close-packed directions, the forward-scattering peaks have substantial elongation, due to the interference discussed before.[16] The brightest and most circular spots are along the close-packed directions ($\theta = 35.3°$). For thicker layers, if the growth switches from fcc to hcp, e.g., from *ABCabca* to *ABCabcb*, the angular profile changes dramatically. The $2 \rightarrow 1$ focusing events always introduce strong new peaks in the $\phi = 60°$ rotated directions, resulting in a pseudosixfold ring. An example for the 4-ML case is shown in Fig. 5, right. Therefore, one can use the appearance of the six bright features at $\theta = 35.3°$ and the lobelike shapes of these features (versus circular spots in the case of fcc stacking)[16] to signal the switchover from fcc to hcp stacking.

In summary, we have shown that angular profiles of high-energy XPS [or Auger electron spectroscopy (AES)] can be used to monitor in detail the stacking sequence in the growth of fcc or hcp Co on Cu(111). For the case of 2 to 3 monolayers, real-space images with lateral resolution of ~ 1 Å can be obtained with the correct orientations and distances. The distances and orientations between nearest-neighbor atoms, together with the focusing directions, can be used to determine three-dimensional structures. The combined use of angular profiles and real-space imaging thus provides valuable three-dimensional structural information even in systems with only local order (i.e., no LEED spots).

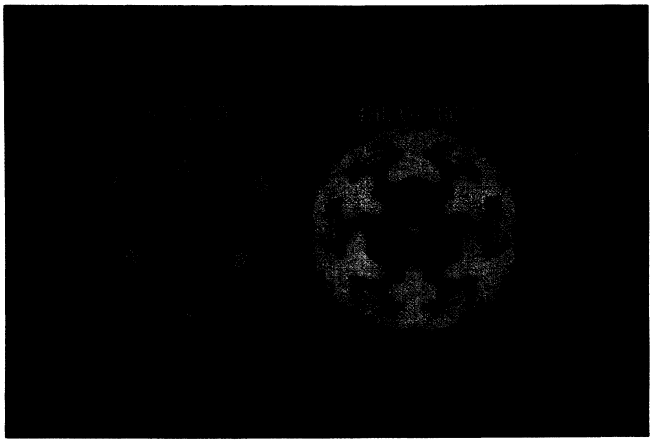

FIG. 5. Angular profiles for 4-ML Co on Cu(111). The "hcp" stacking is *ABCabcb*, corresponding to top layer hcp, deeper layers fcc.

The transition from metastable to bulk phases has been studied by Chambers, Wagner, and Weaver for fcc Fe on Cu(001).[17] They found an order $\rightarrow$ disorder transition at 5 ML or more of fcc Fe. This is expected because the fcc $\rightarrow$ bcc Fe transition is accompanied by substantial change in the lattice constant. The systems studied here, those of fcc $\rightarrow$ hcp Co(111), involve a change in the stacking sequence, but minimal change in the lattice constant. The transition is expected to be order $\rightarrow$ order. In either case, forward-scattering XPS (or AES) is an effective monitoring technique.

This work is supported by the National Science Foundation, Grant No. DMR-8805938, and the Donors of the Petroleum Research Fund, administered by the American Chemical Society.

[1]S. Y. Tong, M. W. Puga, H. C. Poon, and M. L. Xu, in *Chemistry and Physics of Solid Surfaces VI*, edited by R. Vanselow and R. Howe (Springer-Verlag, New York, 1986), pp. 509–545.

[2]W. F. Egelhoff, Jr., Crit. Rev. Solid State Mater. Sci. **16**, 213 (1990).

[3]H. Li and B. P. Tonner, Phys. Rev. B **37**, 3939 (1988).

[4]M. L. Xu and M. A. Van Hove, Surf. Sci. **207**, 215 (1989).

[5]H. Li and B. P. Tonner, Phys. Rev. B **40**, 10241 (1989).

[6]S. A. Chambers, S. B. Anderson, and J. H. Weaver, Phys. Rev. B **32**, 4872 (1985).

[7]C. S. Fadley, in *Synchrotron Radiation Research: Advances in Surface Science*, edited by R. Z. Bachrach (Plenum, New York, 1989).

[8]H. C. Poon and S. Y. Tong, Phys. Rev. B **30**, 6211 (1984).

[9]S. Y. Tong, H. C. Poon, and D. R. Snider, Phys. Rev. B **32**,

2096 (1985).
[10]H. C. Poon, D. R. Snider, and S. Y. Tong, Phys. Rev. B **33**, 2198 (1986).
[11]J. J. Barton, Phys. Rev. Lett. **61**, 1356 (1988).
[12]D. K. Saldin and P. L. de Andres, Phys. Rev. Lett. **64**, 1270 (1990).
[13]S. Y. Tong, C. H. Li, and A. R. Lubinsky, Phys. Rev. Lett. **39**, 498 (1977).
[14]C. H. Li, A. R. Lubinsky, and S. Y. Tong, Phys. Rev. B **17**, 3128 (1978).
[15]C. M. Wei, T. C. Zhao, and S. Y. Tong (to be published).
[16]See, X. D. Wang, Z. L. Han, B. P. Tonner, Y. Chen, and S. Y. Tong, Science **248**, 1129 (1990), for a 15-ML fcc slab of Cu(111).
[17]S. A. Chambers, T. J. Wagner, and J. H. Weaver, Phys. Rev. B **36**, 8992 (1987).

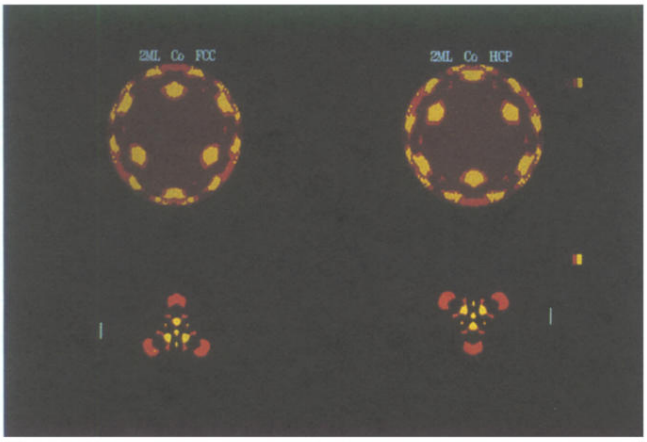

FIG. 1. Angular XPS profiles are shown in the upper panels. The focusing peaks are gold colored. The polar and azimuthal directions are shown in Fig. 2(a). Atomic images are shown in the lower panels, in red color. The vertical white bars equal 1 Å in real space.

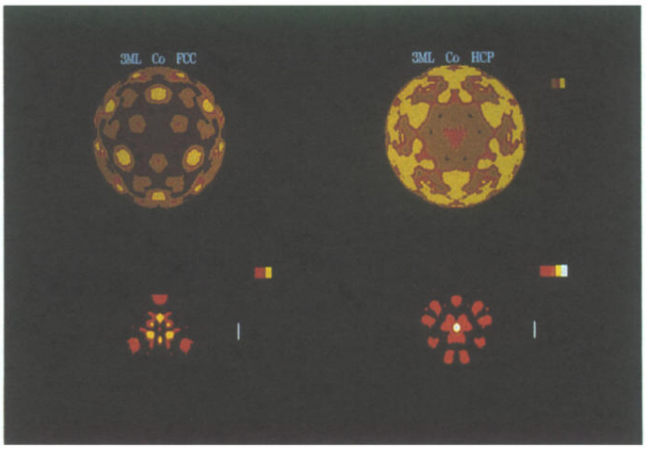

FIG. 3. Angular profiles and real-space images for 3-ML Co on Cu(111). The polar and azimuthal directions are shown in Fig. 2(b). Other conditions same as in Fig. 1.

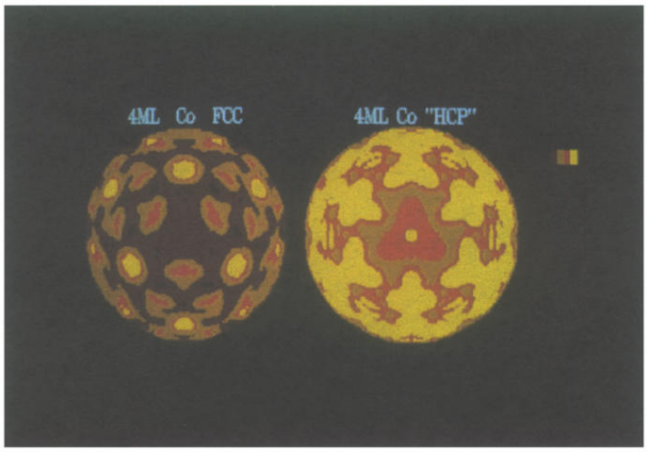

FIG. 5. Angular profiles for 4-ML Co on Cu(111). The "hcp" stacking is *ABCabcb*, corresponding to top layer hcp, deeper layers fcc.